RSC Advances

This is an *Accepted Manuscript*, which has been through the Royal Society of Chemistry peer review process and has been accepted for publication.

Accepted Manuscripts are published online shortly after acceptance, before technical editing, formatting and proof reading. Using this free service, authors can make their results available to the community, in citable form, before we publish the edited article. This *Accepted Manuscript* will be replaced by the edited, formatted and paginated article as soon as this is available.

You can find more information about *Accepted Manuscripts* in the **Information for Authors**.

ROYAL SOCIETY
OF **CHEMISTRY**

www.rsc.org/advances

Facile synthesis of MOF 235 and its superior photocatalytic capability under visible light irradiation

Yingjie Li[a]*, Guangshun Hou[b], Yuan Yang[a], Jin Xie[a], Xiaoli Yuan[a],

Hua Yang[a], Miaomiao Wang[a]

[a] Department of Physics and Chemistry, Henan Polytechnic University, Jiaozuo 454000, P.R.

China

[b] School of Resources and Environment Engineering, Henan Polytechnic University,

Jiaozuo 454000, P.R. China

Abstract: The potential of synthesized MOF 235 crystals using microwave-assisted method was presented, with the advantages of short reaction time and easy procedure obtained. The as-prepared sample (MA-MOF 235) was characterized by powder X-ray diffraction (PXRD), scanning electron microscope (SEM), ultraviolet-visible spectroscopy (UV-vis), fourier transform infrared spectra (FTIR), X-ray photoelectron spectroscopy (XPS) and N_2 adsorption-desorption isotherm. Meanwhile, the photocatalytic activity of the prepared sample for degradation of Rhodamine B (RhB) under visible light irradiation was also investigated. For comparison, the MOF 235 crystals were also prepared by conventional solvothermal method, and the ST-MOF 235 was obtained and characterized. The photocatalytic results show that both

*Corresponding author. Email: liyingjie@hpu.edu.cn. Tel.: (86)391-3987818. Fax:(86)391-3987811.

MA-MOF 235 and ST-MOF 235 exhibit excellent activity for RhB degradation, and they could completely decompose the 40 μmol L^{-1} RhB in the presence of 1 mmol H_2O_2 under visible light irradiation within 20 min. The RhB degradation over both synthesized samples followed first-order kinetics. Moreover, MA-MOF 235 showed a very stable activity for RhB degradation and without significant loss of photocatalytic activity after three consecutive usages. The microwave-assisted method is characterized with speedy, highly efficient and the as-prepared MA-MOF 235 exhibits high visible-light-driven photocatalytic efficiency for organic pollutant degradation in comparison with other MOF-based photocatalysts. Therefore, the as-prepared photocatalyst would have great potential for environmental purification.

Keywords: Microwave-assisted method, MOF 235, Photocatalysis, Hydrogen peroxide, Visible light

With the industrial and social development, contamination of water body and deterioration of water quality has increasingly becoming one of the most serious global environmental issues for human beings [1-3], and extensive research on the advanced technology for the elimination of hazardous chemical compounds has been developed in the past several decades [4-8]. Among various chemical, physical, and

biological technologies in pollution control, photocatalysis has consistently drawn much attention worldwide since it provides the possibility to employing sunlight, which is the most attractive and abundant renewable energy, to promote reactions under very mild conditions [9-12]. Since the demonstration of the first artificial photocatalytic system for organic pollutants degradation over TiO_2 under UV light, several UV-active and visible-response photocatalysts, such as ZnO [13,14], Fe_2O_3 [15,16], CdS [17,18] and ZnS [19,20] have demonstrated efficiency in degrading a wide range of organic pollutants into biodegradable or less toxic organic compounds, even eventually mineralizing them into innocuous CO_2 and H_2O in the gas or aqueous phase. Unfortunately, the low quantum yield and solar energy conversion efficiency of these inorganic photocatalysts limit their practical applications in environmental purification. Therefore, it is highly desirable to search for new photocatalysts with improved performances under visible-light illumination.

Metal-organic frameworks (MOFs), a new class of crystalline molecular solids built from linking organic ligands with metal or metal-cluster connecting points, have generated a rapid development due to their diverse and easily tailored structures, as well as various potential applications in gas storage [21,22], sensing [23,24], separation [25,26], catalysis [27,28], and so on. Recent progress has shown that some MOFs behave as semiconductors under light irradiation [29-32], thus it provides a unique opportunity for integrating different molecular functional components to achieve light harvesting and to drive photocatalytic reaction. MOF-5 was first proposed to behave as a

3

photocatalyst for the photodegradation of phenol by Garcia and co-workers [33], who found that MOF-5 exhibited comparable activity for phenol degradation in the aqueous solutions to that of the commercial TiO_2 (Degussa P-25). Furthermore, MOF-5 displayed reverse shape-selectivity in which large phenolic molecules that cannot access to the interior of MOF-5 degraded much faster than those that can diffuse freely into the micropores of MOF-5. Natarajan and co-workers [34] used a series of MOFs based on Co, Ni, and Zn as photocatalysts to degrade different organic dyes, like orange G, rhodamine B, remazol blue R, and methylene blue. The photocatalytic results show that all three MOFs are active for the photodegradation of the four dyes, and the photocatalytic activities of three MOFs photocatalysts followed a reverse order with respect to their band gap values. Isimjan and coworkers [35] combined the photocatalytic properties of TiO_2 with the strong adsorbing properties of Pt/ZIF-8, and the composite material displayed enhanced catalytic efficiency and better visible light response for the photodegradation of phenol. A doubly interpenetrated porous MOF UTSA-38 with a band gap of 2.85 eV has been used as an UV- or visible- light- driven photocatalyst for the degradation of methyl orange in solution [36]. And more recently, Jiang and coworkers have demonstrated that the iron-based MIL-53(Fe) metal-organic framework shows strong capability toward the activation of H_2O_2 to realize the highly efficient catalytic activity in the degradation of RhB under visible light irradiation [37]. These emerging researches clearly indicate MOFs to be a potential new class photocatalysts for solving environmental issues. However, in contrast to the conventional photocatalysts of metal oxides and sulfides,

the exploration for the photocatalytic properties of MOFs have remained in their

infancy state.

MOF-235 or $[Fe_3O(1,4\text{-}BDC)_3(DMF)_3][FeCl_4](DMF)_3]$ is orange octahedral

single crystals in which each iron atom is trivalent, yielding an overall cationic (+1

per formula unit) framework, and it was first synthesized by Yaghi group in 2005

using a solvothermal method [38]. Recently, MOF 235 is a value-added material for the

adsorption of organic dye in liquid phase [39] and gases adsorption including CH_4, CO_2,

H_2 [40]. To the best of our knowledge, no attention, however, has been paid to study the

photocatalytic property of MOF 235 to date. MOF 235 has been mostly synthesized

by a solvothermal method developed a decade ago. Up to now, microwave-assisted

method has been rapidly developed as an alternative method due to rapid heating,

faster kinetics, homogeneity, better reproducibility and energy saving [41].

In this study, MOF 235 crystals were prepared via a rapid microwave-assisted

method, and the photocatalytic performance of the as-synthesized sample on the

degradation of organic dye was investigated in detail. For comparison, the MOF 235

crystals were also prepared by conventional solvothermal method. Rhodamine B

(RhB) dye, a common organic pollutant, was used as a model to examine the

photocatalytic behavior of the photocatalyst. Compared to the solvothermal method,

this microwave-assisted method offers several advantages including short reaction

time, easy procedure and energy saving. The both synthesized samples exhibit

excellent photocatalytic activity toward the degradation of RhB under visible light

irradiation. With the addition of hydrogen peroxide (H_2O_2), an environmentally benign oxidant, the photocatalytic rate of RhB degradation over MOF 235 prepared by the two methods is accelerate evidently. Moreover, the MA-MOF 235 photocatalyst is highly stable in aqueous solution and could be reused three consecutive cycles without obvious loss of catalytic activity.

2. Experimental

2.1. Materials

$FeCl_3 \cdot 6H_2O$ was purchased from Sinopharm Chemical Reagent Co. Ltd., Shanghai, China. Terephthalic acid (1,4-BDC), H_2O_2 (30%,v/v), dimethylformamide (DMF) and ethanol were supplied by Shanghai Jingchun Industry, Shanghai, China. Rhodamine B (RhB), used as the model pollutant, was obtained from Luoyang Haohua Chemical Reagent Co, Ltd, Luoyang, China. All chemicals and reagents were of analytical grade and used as received without further purification. Doubly distilled deionized water was used throughout this work.

2.2 Synthesis of MOF 235 photocatalyst

2.2.1 Microwave-assisted method

In a typical synthesis, 0.5125 g of terephthalic acid was dissolved in 30 mL DMF solvent and the mixture was stirred for 10 min. And then 0.5000 g of $FeCl_3 \cdot 6H_2O$ was added into the solution and stirred for 10 min, the reactant mixture of 30 mL and 30

mL of ethanol were put in the MD6H microwave reactor (Aplsh, 500W, 2.0 atm) at

100 ^{o}C for 30 min. After cooling down to room temperature, the resulting solid was

collected by centrifugation and washed with DMF-ethanol (1:5, v/v) mixture, and

finally dried in a vacuum at 150 ^{o}C for 5 h, and the final MA-MOF 235 photocatalyst

was obtained.

2.2.2   Solvothermal method

MOF 235 was synthesized by a solvothermal method as reported previously with

minor modification [39]. 0.1025 g terephathalic acid was disssolved in 30 mL DMF, and

the mixture was stirred for 10 min till a clear solution was formed. Then, 0.1000 g

FeCl$_3$·6H$_2$O was added into the solution with continuous stirring for 10 min.

Subsequently, 30 mL of the reaction solution and 30 mL ethanol were transferred into

100 mL Teflon-lined stainless autoclave and heated at 80 ^{o}C for 24 h. After cooling

down, the orange crystals were collected by centrifugation and were washed with

DMF-ethanol (1:5, v/v) mixture after being kept at 150 ^{o}C for 15 h, and the final

ST-MOF 235 photocatalyst was obtained.

2.3   Characterization

The X-ray diffraction (XRD) patterns were performed on a D8 Advance

diffractometer (Bruker) with Cu Kα radiation (40kV, 40mA). The surface morphology

and size of MOF 235 products were observed by field emission scanning electron

microscopy (FEI Quanta 250) and operating at 20 kV. Fourier transformation infrared

(FT-IR) spectra was acquired in the range $450 \sim 4000$ cm^{-1} with a Bruker V70 FT-IR spectrophotometer using KBr and sample mixture pellets. UV-vis diffuse reflectance spectra (UV-vis DRS) were measured over the spectral range $210 \sim 720$ nm with a spectrophotometer (UV-4100, Hitachi) using $BaSO_4$ as reflectance standard. X-ray photoelectron spectroscopy (XPS) measurements were performed on a Thermo ESCALAB 250Xi system with Mg Kα source. All the binding energies were calibrated by C 1s peak at 284.8 eV of the surface adventitious carbon. Total organic carbon (TOC) was carried out on a Tekmar Dohrmann Apollo 9000 TOC analyzer.

2.4   Photocatalytic activity measurement

The photocatalytic activity of the MOF 235 photocatalyst was evaluated by photodegradation of RhB dye using visible light at room in open air and at room temperature. In a typical run, 10 mg of MOF 235 photocatalyst was added into 50 mL of RhB aqueous solution (40 μmol L^{-1}) in a 100 mL beaker. Afterwards, the suspension was magnetically stirred in the dark for 30 min to ensure the adsorption - desorption equilibrium, followed by the addition of 1 mmoL of H_2O_2 to the mixture solution. The suspension was then illuminated by a 300 W xenon lamp (PLS-SXE 300, China), all the radiation with wavelength shorter than 420 nm was removed by a cutoff filter. During the irradiation procedure, stirring was maintained to keep the mixture in suspension, and 5 mL of suspension was withdrawn at regular intervals and centrifuged to remove photocatalyst particles for analysis. The concentration of RhB left in the supernatant solution was determined by measuring the absorption intensity

at its maximum absorbance wavelength of λ = 554 nm using a UV-visible

spectrophotometer (Evolution 201, Thermo Scientific).

3. Results and Discussions

3.1. Characterization

The crystallographic structure of the as-prepared products were first characterized

by powder X-ray diffraction (PXRD). As can be seen from Fig.1, the samples

obtained using microwave-assisted method (Fig.1a) and solvothermal method (Fig.1b)

show almost the same diffraction patterns, clearly suggesting the MOF 235 crystals

prepared by the two synthetic methods are isostructural. The main diffraction peaks

were at 2θ = 9.7, 12.6, 19 and 22, which are in good agreement with the previously

reported MOF 235 as well as the simulated one (Fig.1c). MOF 235 crystals obtained

in this work display relatively weak diffraction peaks in comparison with the products

prepared by Yaghi and coworkers [38]. The weak diffraction peaks could be attributed to

the crystalline size of the as-prepared MOF crystals is smaller than that obtained by

the Ref. [38] (37 - 42 μm), and further confirmed by scanning electron microscope

(SEM) investigations as shown below. No impurity peaks were detected in the PXRD

pattern, indicating that the obtained products are single phase MOF 235 photocatalyst.

To gain a better understanding of the morphology and particle size of the

MA-MOF 235 crystals synthesized by microwave-assisted method, the sample was

also characterized using SEM (Fig.2). Fig. 2a is low magnification SEM image of the

synthesized MA-MOF 235. Clearly, the as-prepared MA-MOF 235 photocatalysts are

well-crystallized octahedral morphology and the size distribution of these crystals is relatively uniform with few exceptions. The magnified SEM image in Fig. 2b reveals that the particle size distribution of 3 - 4.5 μm were dominative for MA-MOF 235 crystals.

Fourier transform infrared spectroscopy (FTIR) spectra was performed in order to deeply analyze the molecular structure and identify the organic function-groups of MA-MOF 235 sample, and the corresponding result is shown in Fig.3. As presented in Fig. 3, the broad peak centered at 3440 cm^{-1} is usually attributed to the stretching vibrations of the O-H from the surface adsorbed water. The weak peak at 2931 cm^{-1} corresponds to C-H stretching vibration of the ligated DMF. The characteristic absorption peaks of the MA-MOF 235 sample were observed at 1663, 1597, 1398, 1016 and 750 cm^{-1}, which could mainly originate from carboxylate groups vibrations and are consistent with those of reported data in the literatures [40]. The two sharp peaks at 1597 and 1398 cm^{-1} can be ascribed to asymmetric (v_{as} (C-O)) and symmetric (v_s (C-O)) vibrations of carboxyl groups, respectively, suggesting the presence of the dicarboxylate linker within the sample. The peak at 750 cm^{-1} results from C-H bending vibrations of the benzene ring. The results confirmed that the compound has been MOF 235.

In order to obtain the information of specific surface area and porous structure of the as-synthesized samples, the N_2 adsorption-desorption isotherms of MA-MOF 235 and ST- MOF 235 were measured at 77 K, and the results are presented in Fig.4. The

N_2 adsorption isotherms on MOF-235 synthesized by the two methods are of a typical type I isotherm, a signature characteristic of microporous materials. According to the Brunauer-Emmett-Teller (BET) equation, the BET surface area and total pore volume of MA-MOF 235 were 148 m^2 g^{-1} and 0.075 cm^3 g^{-1}, which were slightly higher than that obtained by ST-MOF 235 (135 m^2 g^{-1} and 0.067cm^3 g^{-1}).

The optical property of the as-prepared samples by the two methods were investigated by UV-vis diffuse reflectance spectroscopy, and the experimental results are shown in Fig. 5. As can be seen, the MOF 235 samples display strong and wide adsorption in the visible light region above 400 nm, and the main optical absorption band is around 650 nm for MA-MOF 235 and 640 nm for ST-MOF 235. These optical transitions can be assigned to ligand-to metal charge transfer (LMCT). Furthermore, the band gap energy can be estimated from a plot of the intercept of the tangents to the plot of $(\alpha h\nu)^{1/2}$ versus photon energy $h\nu$. As observed in the inset of Fig. 5, The band gap energies of MA-MOF 235 and ST-MOF 235 were estimated to be 1.94 eV and 1.98 eV, which are both lower than Eg values of TiO_2 (3.2 eV) [42] and g-C_3N_4 (2.7 eV) [43], suggesting that MOF 235 crystallines could sufficiently absorb visible light and may possess good photocatalytic properties when irradiated under visible light.

X-ray photoelectron spectroscopy (XPS) analysis was performed to investigate the surface composition and chemical states of as-synthesized samples, as shown in Fig.6. High- resolution XPS spectra of Fe 2p (Fig.6A) show the binding energy peaks is around 711.6 eV and 725.6 eV, which are attributed to Fe $2p_{3/2}$ and Fe $2p_{1/2}$,

respectively. The peak separation, namely, $\Delta = 2p_{1/2}-2p_{3/2} = 14$ eV, is very similar to

those reported for Fe_2O_3, indicating that the two peaks belong to Fe^{3+} of the MOF 235

prepared by the two methods. Furthermore, Fig.6 B, C and D also show the XPS

patterns of MA-MOF 235 are similar to that of ST-MOF 235, suggesting the chemical

environments of Fe^{3+} are identical in MOF 235 samples prepared by the two methods.

Before light irradiation, the suspension including MOF 235 and RhB was

magnetically stirred in the dark to establish an adsorption-desorption equilibrium

between the pollutants and the surface of the photocatalysts. The result shows that

MOF 235 can speedy get to the adsorption-desorption equilibrium state in 30 min.

The photocatalytic degradation of RhB was used to evaluate the catalytic performance

of as-synthesized samples. The photocatalytic activity of the MOF 235 was monitored

in terms of the RhB color change by measuring its maximum absorbance at $\lambda_{max} = 554$

nm. Control experiments without photocatalyst and light irradiation were also

performed. Fig. 7 shows the normalized concentration of RhB (C/C_0) against the

reaction time during various processes. It can be seen that the degradation of RhB was

negligible after 40 min visible light irradiation in the absence of the catalyst (Fig. 7a),

clearly demonstrating that RhB is relatively stable under visible light irradiation. In

contrast, after the addition of the catalysts, the degradation efficiency of RhB were 9.4%

for MA-MOF 235 (Fig. 7b) and 9.2% for ST-MOF 235 (Fig. 7c) after 40 min visible

light irradiation, indicating that the both synthesized samples show the photocatalytic

activity for RhB degradation, although the photodegradation rate is low. The reaction

mechanism for RhB degradation could be discussed based on the semiconductor

12

theory. In the presence of light with adequate energy, electron (e$^-$) can be excited from VB of MOF 235 to enter into its CB and produce holes (h$^+$) in the VB. The photogenerated holes with strong oxidation ability could directly oxidize adsorbed organic molecules, and the resulting hydroxyl radical (•OH) could also decompose RhB molecules that were adsorbed on the surface of MOF 235 particles. Meanwhile, molecular oxygen can trap photogenerated electrons (e$^-$) to form superoxide radical (•O$_2^-$), which also possesses a strong oxidant ability to decolorize the RhB molecules. The low efficiency of RhB photodegradation over MOF 235 photocatalyst could be attributed to the fast electron-hole recombination. Therefore, the introduction of external electron acceptor (such as H$_2$O$_2$) is expected to hinder the electron-hole recombination and enhance the performance of MOF 235 photocatalyst. The control experiment was also conducted by irradiating the RhB aqueous solution containing H$_2$O$_2$ additive in the absence of MOF 235 under visible light. About 8.6% RhB was degraded when only H$_2$O$_2$ was used in the reaction after 40 min of visible light irradiation (Fig.7d). In view of the photocatalyst is iron-based MOF, the Fenton-like catalytic process could also induce the RhB degradation in the presence of H$_2$O$_2$, therefore, the control experiment by combination of H$_2$O$_2$ and MOF 235 without light irradiation was further carried out. As a result, in the presence of catalyst and H$_2$O$_2$ without light irradiation, the degradation efficiency of RhB were 14.1% for MA-MOF 235 (Fig. 7e) and 13.1% for ST-MOF 235 (Fig. 7f). However, with the addition of H$_2$O$_2$ and MOF 235 simultaneously, the degradation efficiency of RhB under visible light irradiation was remarkbly enhanced, it could completely decompose the RhB

within 20 min (Fig. 7g and h). The result shows that the degradation efficiency in such Fenton-like catalytic process just as MOF 235/H_2O_2 was relatively much lower than that in MOF 235/H_2O_2/visible light catalytic system.

To achieve a better understanding of the reaction kinetics of the RhB degradation catalyzed by various catalytic systems, the experimental data was fitted by a pseudo-first-order model. Fig.8 indicates a linear relationship between $\ln(C/C_0)$ and the irradiation time for RhB degradation. The values of rate constant (k) can be calculated from the slope and the intercept of the linear plot. As shown in Fig.8, the rate constants for the MA-MOF 235/ visible light, ST-MOF 235/ visible light, H_2O_2/ visible light, MA-MOF 235/ H_2O_2 catalytic system and ST-MOF 235/ H_2O_2 catalytic system were 0.0025, 0.0024, 0.0023, 0.0039 and 0.0035 min^{-1}, respectively. The kinetic enhancement of the catalyzed degradation of RhB in MOF 235/ H_2O_2/ visible light catalytic system was achieved, and the rate constant of 0.254 min^{-1} for MA-MOF 235 was slightly higher than obtained by ST-MOF 235 (0.243 min^{-1}). Furthermore, both of them were found to be much higher than that of the sum of MOF 235/visible light and H_2O_2/visible light catalytic systems, which indicates the synergic effect of MOF 235 photocatalyst, H_2O_2 and visible light irradiation in the photocatalytic process could contribute cooperatively to the whole catalytic activity for the degradation of RhB. The synergy index (SI), defined as SI=K ($_{H2O2+MOF235}$)/($K_{H2O2}+K_{MOF235}$), is 52.9 for MA-MOF 235 and 51.7 for ST-MOF 235, indicating a pronounced synergic effect with the electron acceptor addition.

As mentioned above, the addition of H_2O_2 was necessary for improving the photocatalytic activity of the MOF 235 photocatalyst, therefore, the effect of H_2O_2 dosage on RhB degradation over MA-MOF 235/ H_2O_2/visible light system was investigated by varying the amount of H_2O_2 under a given reaction condition and the results are shown in Fig.9. When the amount of H_2O_2 increased from 0.5 to 1 mmol, the degradation rate increased correspondingly from 0.082 to 0.254 min^{-1}, and the degradation rate was kept constant with the further increase of H_2O_2 dosage to 4 mmol. The enhanced photocatalytic MB degradation rate with the H_2O_2 addition should be attributed to the scavenging of the excited electrons from MOF 235 by H_2O_2, leading to efficient suppression of the electron- hole recombination, so that the photogenerated holes can generate more ·OH radicals, thus enhancing the photocatalytic RhB degradation rate.

In order to study the mineralization of dye over MA-MOF 235, total organic carbon (TOC) was carried out and the result is depicted in Fig.10. TOC determination indicated that the extent of RhB mineralization increased with the increase of irradiation time. After 20-min of irradiation, above 98% of TOC was removed from the bulk solution, which suggests the facile mineralization of RhB in the MOF 235/H_2O_2/visible light catalytic system, and the dye should be degraded into carbon dioxide.

The stability and reusability of photocatalyst is very important issues for practical applications. For this purpose, recycling reactions were carried out for the

15

photodegradation of RhB over MA-MOF 235/H_2O_2/visible system. In each test, the photocatalyst was reused after washing with ethanol and dried at 80 ^{o}C while other factors were kept identical. Fig.11 shows the time course of RhB decolorization during three consecutive cycles. It showed that the catalytic performance of the MOF 235 catalyst remained almost unchanged after three recycles for degradation of RhB, indicating that the MOF 235 catalyst is considerably stable during the photodegradation of the dyes.

Fig. 12 shows the Fe 2p binding energy spectra of MA-MOF 235 before and after repeated usages. As it can be seen, there was no significant variation of the XPS data after repeated use for three cycles, further indicating good stability of MOF 235 as a photocatalyst. Moreover, the atomic absorption spectrometer (AAS; TAS- 990, Purkinje General, P. R. China) analysis reveals that only a trace amount of Fe ions was detected in the centrifuged solution after three cycle usages.

For comparison, the performances obtained by MA-MOF 235 with other MOF-based materials as photocatalysts for the degradation of organic pollutants in aqueous media under visible light irradiation are also shown in Table 1. As could be seen: (1) the synthesis time of MA-MOF 235 is much shorter than that reported in Refs. 31, 37, 44 and 45; (2) the degradation efficiency obtained by MA-MOF 235 is higher than that reported in Refs. 31 (Cu(ptz)(II)), 44 and 45, and is comparable with Refs. 31 (Cu(ptz)(I)) and 37.

Conclusion

In summary, we have developed a rapid and facile microwave- assisted synthesis method for preparing iron-based MOF 235 photocatalyst (MA-MOF 235) and evaluated in terms of performance by degradation of RhB aqueous solution under visible light irradiation. For comparison, the MOF 235 crystals are also prepared by conventional solvothermal method. The photodegradation of RhB over both synthesized samples followed first-order kinetics, and the rate constant of MA-MOF 235 photocatalyst is 0.0025 min^{-1} for visible light irradiation. Remarkbly, the MA-MOF 235 catalyst exhibits excellent photocatalytic activity for degradation of RhB under visible light irradiation in the presence of H_2O_2, the rate constant of 0.254 min^{-1} was achieved. The enhanced photocatalytic activity for degradation of RhB is attributed to the cooperative effects of MOF 235 photocatalyst, H_2O_2 and visible light irradiation. Moreover, MA-MOF 235 displays a high chemical stability for repeated RhB degradation reactions. This work provides new insights on simplifying synthesis and further demonstrates the great potential of MOFs to be powerful photocatalysts for environmental remediation.

Acknowledgments

References

1   K. M. Tedd, C. E. Coxon, B. D. Misstear, D. Daly, M. Craig, A. Mannix and N. H. Williams, *Sci. Total. Environ.*, 2014, 476-477, 460- 476.

2   P. N. Palanisamy and S. K. *Kavitha, India, E-J. Chem.*, 2010, 7, 1033- 1039.

3   X.-L. Wang, J.-Y. Han, L.-G. Xu and Q. Zhang, *Environ. Pollut.*, 2010, 158, 1513- 1520.

4   W.-X. Qi, H. Singer, M. Berg, B. Müller, B. Pernet-Coudrier, H.-J. Liu and J.-H. Qu, *Chemosphere*, 2015, 119, 1054- 1061.

5   B. Gargouri, O. D. Gargouri, B. Gargouri, S. K. Trabelsi, R. Abdelhedi and M. Bouaziz, *Chemosphere*, 2014, 117, 309- 315.

6   M. Kiel, D. Dobslaw and K. H. Engesser, *Water Res.*, 2014, 66, 1- 11.

7   J.-W. Hou, G.-X. Dong, Y. Ye and V. Chen, *J. Membrane Sci.*, 2014, 469, 19- 30.

8   C. K. C. Araujo, G. R. Oliveira, N. S. Fernandes, C. L. P. S. Zanta, S. S. L. Castro, D. R. da Silva and C. A. Martinez-Huitle, *Environ. Sci. Pollut. Res.*, 2014, 21, 9777- 9784.

9   D.-L. Feng, S.-H. Xu and G. Liu, *Chemosphere*, 2015, 125, 102- 107.

10   Y.-B. He, D. Langsdorf, L. Li and H. Over, *J. Phys. Chem. C*, 2015, 119, 2692- 2702.

11   P. Lei, F. Wang, S.-M. Zhang, Y.-F. Ding, J.-C. Zhao and M.-S. Yang, *Appl. Mater. Interfaces*, 2014, 6, 2370- 2376.

12   X.-J. Lang, W.-H. Ma, C.-C. Chen, H.-W. Ji and J.-C. Zhao, *Acc. Chem. Res.*, 2014, 47, 355- 363.

13   N. T. Khoa, S. W. Kim, D. H. Yoo, S. Cho, E. J. Kim and S. H. Hahn, *Appl. Mater. Interfaces*, 2015, 7, 3524- 3531.

14   L.-X. Song, Q.-X. Jiang, P.-F. Du, Y.-F. Yang and J. Xiong, *Mater. Lett.*, 2014, 123, 214- 216.

15   X.-L. Cheng, J.-S. Jiang, C.-Y. Jin, C.-C. Lin, Y. Zeng and Q.-H. Zhang, *Chem. Eng. J.*, 2014, 236, 139- 148.

16   S.-L. Bai, K.-W. Zhang, J.-H. Sun, R.-X. Luo, D.-Q. Li and A.-F. Chen, *CrystEngComm*, 2014, 16, 3289- 3295.

17   Q.-Y. Liu, J. Li, Y.-Q. Zhao, Y. Zhou and C.-R. Li, *Mater. Lett.*, 2015, 138, 89- 91.

18   R. Bera, S. Kundu and A. Patra, *Appl. Mater. Interfaces*, 2015, 7, 13251- 13259.

19   K. R. Raksha, S. Ananda, N. M. Madegowda, *J. Mol. Catal. A: Chem.*, 2015,

396, 319- 327.

20 D.-G. Chen, F. Huang, G.-Q. Ren, D.-S. Li, M. Zheng, Y.-J. Wang and Z. Lin, *Nanoscale*, 2010, 2, 2062- 2064.

21 B. Borah, H.-D. Zhang and R.-Q. Snurr, *Chem. Eng. Sci.*, 2015, 124, 135- 143.

22 L.-J. Li, J. G. Bell, S.-F. Tang, X.-X. Lv, C. Wang, Y.-L. Xing, X.-B. Zhao and K. M. Thomas, *Chem. Mater.*, 2014, 26, 4679- 4695.

23 J.-S. Cui, Y.-L. Wong, M. Zeller, A. D. Hunter and Z.-T. Xu, *Angew. Chem. Int. Ed.*, 2014, 53, 14438- 14442.

24 Y.-N. Gong, Y.-L. Huang, L. Jiang and T.-B. Lu, *Inorg. Chem.*, 2014, 53, 9457- 9459.

25 S. Yang, A. J. Ramirez-Cuesta, R. Newby, V. Garcia-Sakai, P. Manuel, S. K. Callear, S. I. Campbell, C.-C. Tang and M. Schroder, *Nat. Chem.*, 2014, 7, 121- 129.

26 T. Rodenas, I. Luz, G. Prieto, B. Seoane, H. Miro, A. Corma, F. Kapteijn, F. X. Llabrés i Xamena and J. Gascon, *Nat. Mater.*, 2015, 14, 48- 55.

27 C. M. McGuirk, M. J. Katz, C. L. Stern, A. A. Sarjeant, J. T. Hupp, O. K. Farha and C. A. Mirkin, *J. Am. Chem. Soc.*, 2015, 137, 919- 925.

28 M. Zhao, S. Ou and C.-D. Wu, *Acc. Chem. Res.*, 2014, 47, 1199- 1207.

29   C. G. Silva, A. Corma and H. García, *J. Mater. Chem.*, 2010, 20, 3141- 3156.

30   R. Li, J.-H. Hu, M.-S. Deng, H.-L. Wang, X.-J. Wang, Y.-L. Hu, H.-L. Jiang, J. Jiang, Q. Zhang, Y. Xie and Y.-J. Xiong, *Adv. Mater.*, 2014, 26, 4783-4788.

31   T. Wen, D.-X. Zhang and J. Zhang, *Inorg. Chem.*,2013, 52, 12-14.

32   C.-C. Wang, J.-R. Li, X.-L. Lv, Y. -Q. Zhang and G.-S. Guo, *Energy Environ. Sci.*, 2014, 7, 2831-2867.

33   F. X. L. I. Xamena, A. Corma and H. Garcia, *J. Phys. Chem. C*, 2007, 111, 80- 85.

34   P. Mahata, G. Madras and S. Natarajan, *J. Phys. Chem. B*, 2006, 110, 13759-13768.

35   T. T. Isimjan, H. Kazemian, S. Rohani and A. K. Ray, *J. Mater. Chem.*, 2010, 20, 10241- 10245.

36   M. C. Das, H. Xu, Z.-Y. Wang, G. Srinivas, W. Zhou, Y.-F. Yue, V. N. Nesterov, G.-D. Qian and B.-L. Chen, *Chem. Commun.*, 2011, 47, 11715-11717.

37   L.-H. Ai, C.-H. Zhang, L.-L. Li and J. Jiang, *Appl. Catal.*, *B* 2014, 148-149, 191- 200.

38   A. C. Sudik, A. P.Côté and O. M. Yaghi, *Inorg. Chem.*, 2005, 44, 2998- 3000.

39   E. Haque, J. W. Jun and S. H. Jhung, *J. Hazard. Materials*, 2011, 185, 507-

511.

40   M. Anbia, V. Hoseini and S. Sheykhi, *J. Ind. Eng. Chem.*, 2012, 18, 1149-

1152.

41   X.-L. Hu, J.-C. Yu, J.-M. Gong, Q. Li, G.- S. Li, *Adv. Mater.* 2007, 19, 2324 –

2329.

42   J. Yang, X.-H. Wang, J. Dai and J.-T. Li, *Ind. Eng. Chem. Res.*, 2014, 53,

12575- 12586.

43   G.-Z. Liao, S. Chen, X. Quan, H.-T. Yu and H.-M. Zhao, *J. Mater. Chem.*,

2012, 22, 2721- 2726.

44   Y.-L. Hou, R. W.-Y. Sun, X.-P. Zhou, J.-H. Wang and D. Li, *Chem.Commun.*,

2014, 50, 2295-2297.

45   J.-W. Ran, S.-W. Liu, P. Wu and J. Pei, *Chin.Chem.Lett.*, 2013, 24, 373-375.

Caption to Figures

Fig.1 PXRD patterns of the MA-MOF 235: (a) synthesized by microwave- assisted method, (b) synthesized by solvothermal method, (c) simulated from the MOF 235 crystal structure data.

Fig. 2 SEM images of the MA-MOF 235.

Fig. 3 FTIR spectra of the MA-MOF 235.

Fig.4 Nitrogen adsorption- desorption isotherms of MA- MOF 235 (a) and ST- MOF 235 (b).

Fig. 5   UV-visible absorption spectra of MA- MOF 235 (a) and ST- MOF 235 (b). The inset shows the corresponding plots of transformed Kubelka-Munk vs energy of light for the photocatalysts.

Fig. 6   (A) Fe 2p XPS spectra of MA- MOF 235 (a) and ST- MOF 235 (b). (B) O 1s XPS spectra of MA- MOF 235 (a) and ST- MOF 235 (b). (C) C 1s XPS spectra of MA- MOF 235 (a) and ST- MOF 235 (b). (D) N 1s XPS spectra of MA- MOF 235 (a) and ST- MOF 235 (b).

Fig.7 Degradation of RhB over the MOF 235 photocatalysts under different catalytic conditions, (a) RhB self-decolorization under visible light irradiation; (b) using MA-MOF 235 as the photocatalyst under visible light irradiation; (c) using ST- MOF 235 as the photocatalyst under visible light irradiation; (d) only with the addition of the H_2O_2 electron acceptor; (e) using MA-MOF 235 photocatalyst and H_2O_2 without light

irradiation; (f) using ST-MOF 235 photocatalyst and H_2O_2 without light irradiation; (g) using MA-MOF 235 photocatalyst and H_2O_2 under visible light irradiation; (h) using ST-MOF 235 photocatalyst and H_2O_2 under visible light irradiation.

Fig.8 The reaction kinetics of RhB over the MOF 235 photocatalyst under different catalytic conditions, (a) using MA- MOF 235 as the photocatalyst under visible light irradiation; (b) using ST- MOF 235 as the photocatalyst under visible light irradiation; (c) only with the addition of the H_2O_2 electron acceptor; (d) using MA-MOF 235 photocatalyst and H_2O_2 without light irradiation; (e) using ST-MOF 235 photocatalyst and H_2O_2 without light irradiation; (f) using MA-MOF 235 photocatalyst and H_2O_2 under visible light irradiation; (g) using ST-MOF 235 photocatalyst and H_2O_2 under visible light irradiation.

Fig.9 Photodegradation of RhB with MOF 235 phocatalyst in the presence of various amounts of H_2O_2 under visible light. (a) 0.5 mmol H_2O_2; (b) 1 mmol H_2O_2; (c) 2 mmol H_2O_2; (d) 4 mmol H_2O_2.

Fig.10 TOC removal yield of degraded bulk solution during the photocatalytic degradation of RhB under visible light.

Fig.11 The photocatalytic RhB decolorization during three consecutive runs over MA-MOF 235/H_2O_2/visible light system.

Fig.12 XPS spectrum of MA-MOF 235 (a)before and (b)after repeated usages for RhB degradation.

Table 1 Comparison of the performances of MOF-based materials as photocatalysts for the degradation of organic pollutants in aqueous media under visible light irradiation

MOF[a]	Synthesis methods	Synthesis conditions	organic pollutants	Initial concentration ($\mu mol\ L^{-1}$)	Time (min)	Degradation efficiency (%)	Ref.
MIL-53(Fe)	Solvothermal	150°C, 2 h	RhB (H$_2$O$_2$)	20.9	50	100	37
Cu(ptz)(I)[b]	Solvothermal	160°C, 72 h	RhB (H$_2$O$_2$)	39.0	35	100	31
Cu(ptz)(II)[b]	Solvothermal	160°C, 72 h	RhB (H$_2$O$_2$)	39.0	35	70[c]	31
[Cu^{II}(salImcy)] (Cu^{I}I)$_2$·DMF	Solvothermal	100°C, 12 h	RhB (H$_2$O$_2$)	25.1	50	95	44
Fe$_2$(bhbdh)	Slow evaporation	One week	RhB (H$_2$O$_2$)	40	15	90	45
MA-MOF 235	microwave-assisted	100 °C, 0.5h	RhB (H$_2$O$_2$)	40	20	100	This work

[a] ptz = 5-(3-pyridyl)tetrazole; salimcy =N, N'-bis-[(imidazol-4-yl)methy- lene] cyclohexane -1,2-diamine; DMF = dimethylformamide; bhbdh = bis[2-hydroxy benzaldehyde]hydrazone. [b] Cu(ptz)(I) and Cu(ptz)(II) are isomers. [c] Value estimated

from original figures of the reference.
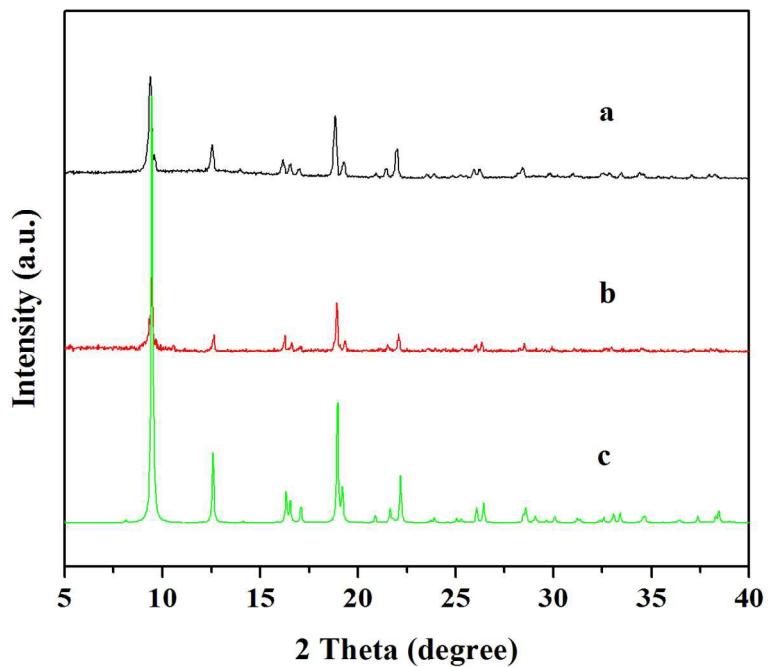
Fig.1 PXRD patterns of the MA-MOF 235: (a) synthesized by microwave- assisted method, (b) synthesized by solvothermal method, (c) simulated from the MOF 235 crystal structure data.
279x215mm (150 x 150 DPI)
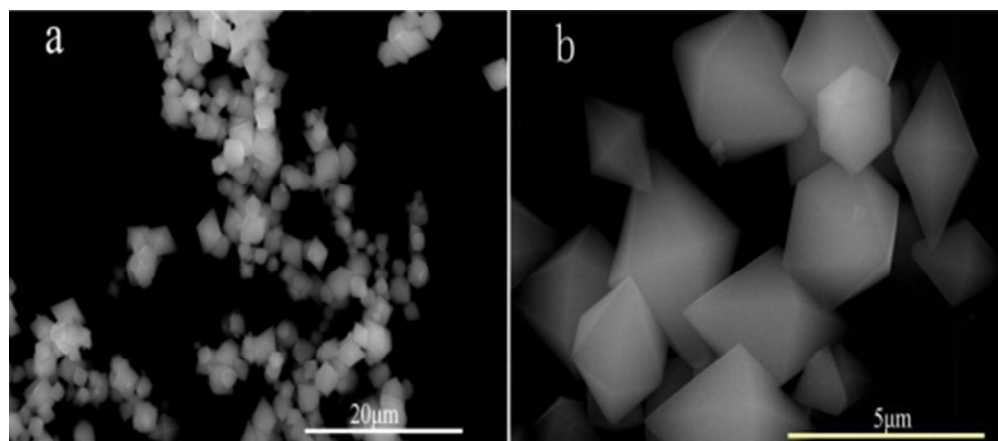
Fig. 2 SEM images of the MA-MOF 235.
138x60mm (96 x 96 DPI)
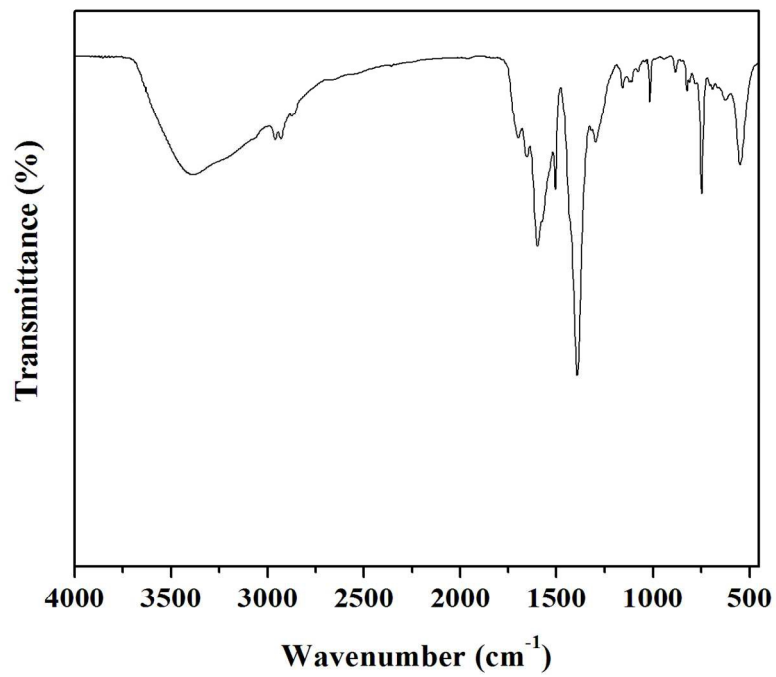
Fig. 3 FTIR spectra of the MA-MOF 235.
279x215mm (150 x 150 DPI)
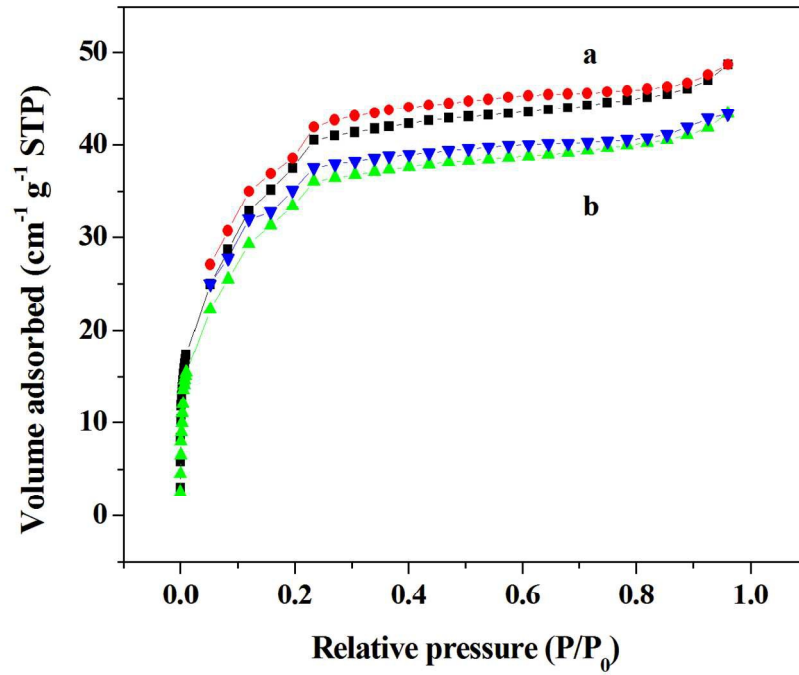
Fig.4 Nitrogen adsorption- desorption isotherms of MA- MOF 235 (a) and ST- MOF 235 (b).
279x215mm (150 x 150 DPI)
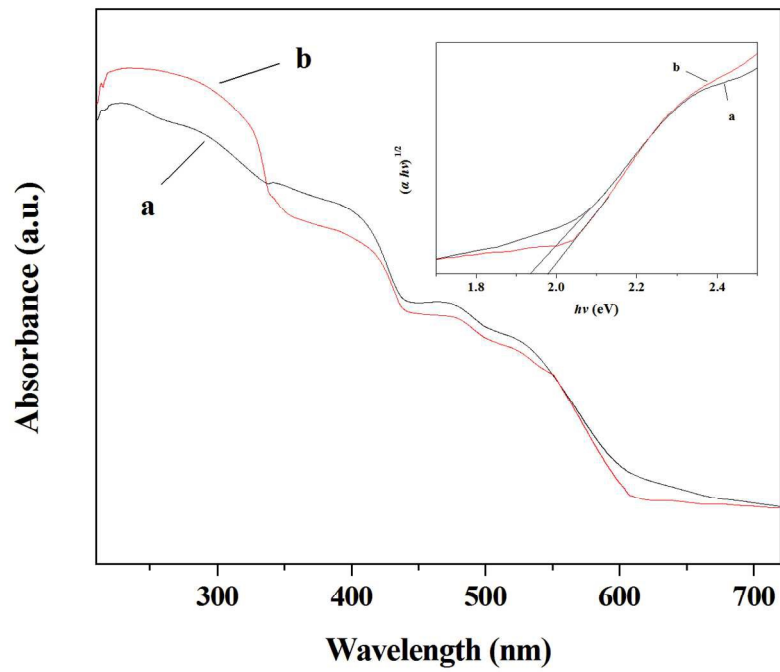
Fig. 5 UV-visible absorption spectra of MA- MOF 235 (a) and ST- MOF 235 (b). The inset shows the corresponding plots of transformed Kubelka-Munk vs energy of light for the photocatalysts.
279x215mm (150 x 150 DPI)
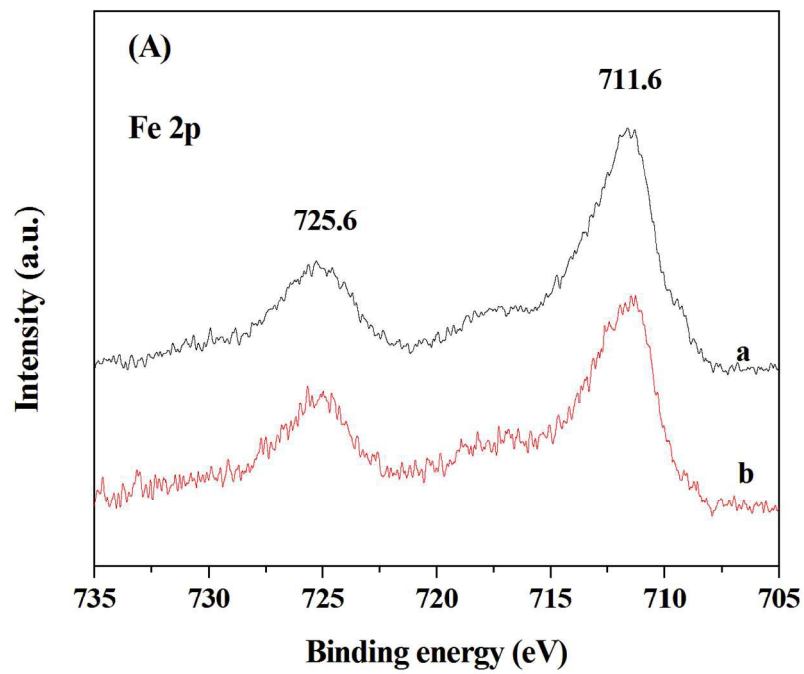
Fig. 6 (A) Fe 2p XPS spectra of MA- MOF 235 (a) and ST- MOF 235 (b).
279x215mm (150 x 150 DPI)
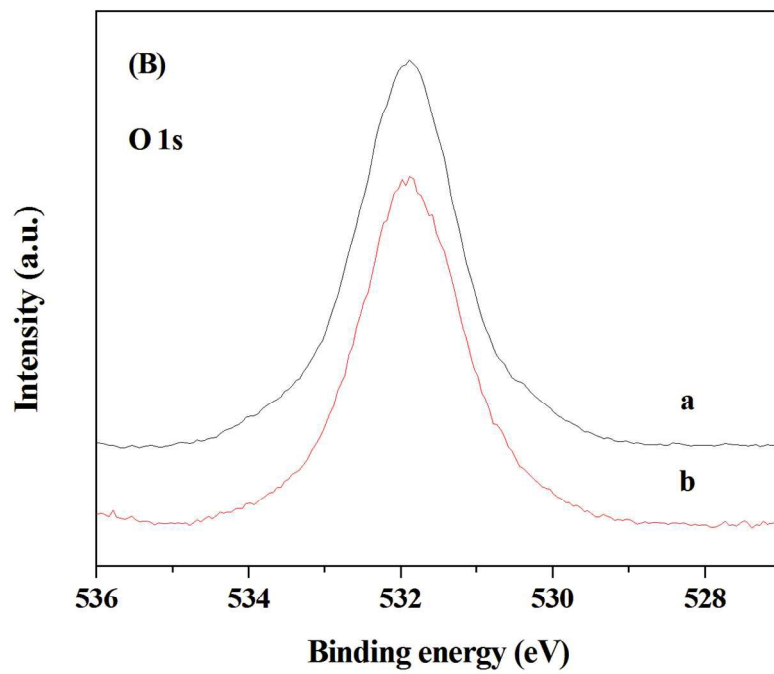
Fig. 6 (B) O 1s XPS spectra of MA- MOF 235 (a) and ST- MOF 235 (b).
279x215mm (150 x 150 DPI)
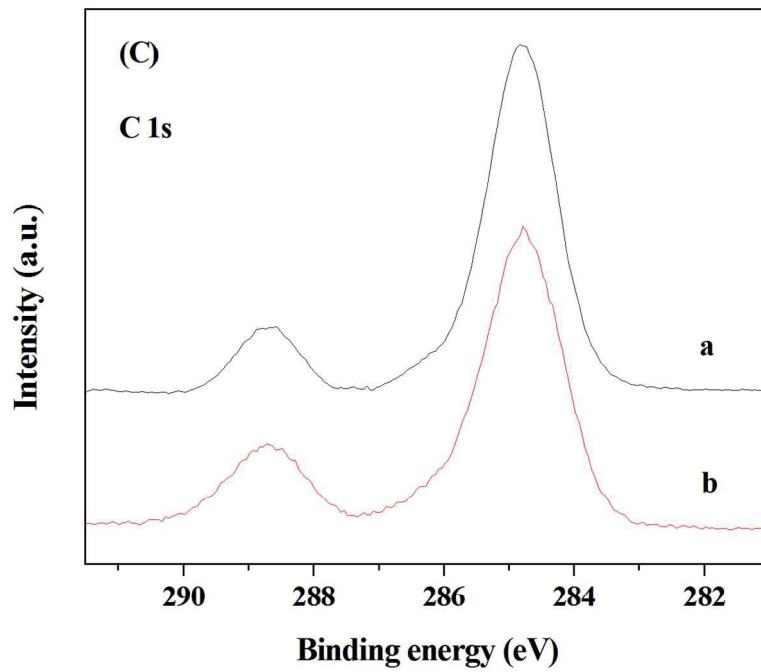
Fig. 6 (C) C 1s XPS spectra of MA- MOF 235 (a) and ST- MOF 235 (b).
279x215mm (150 x 150 DPI)
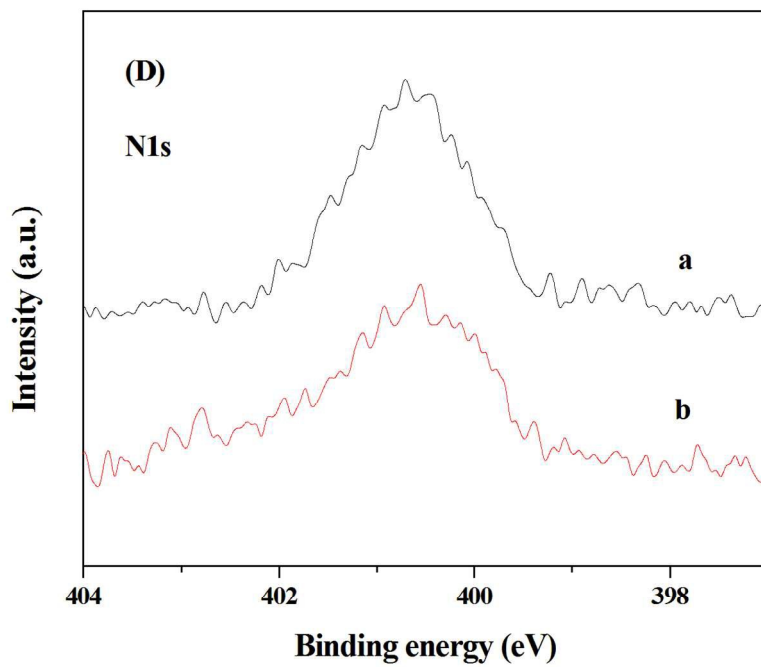
Fig. 6 (D) N 1s XPS spectra of MA- MOF 235 (a) and ST- MOF 235 (b).
279x215mm (150 x 150 DPI)
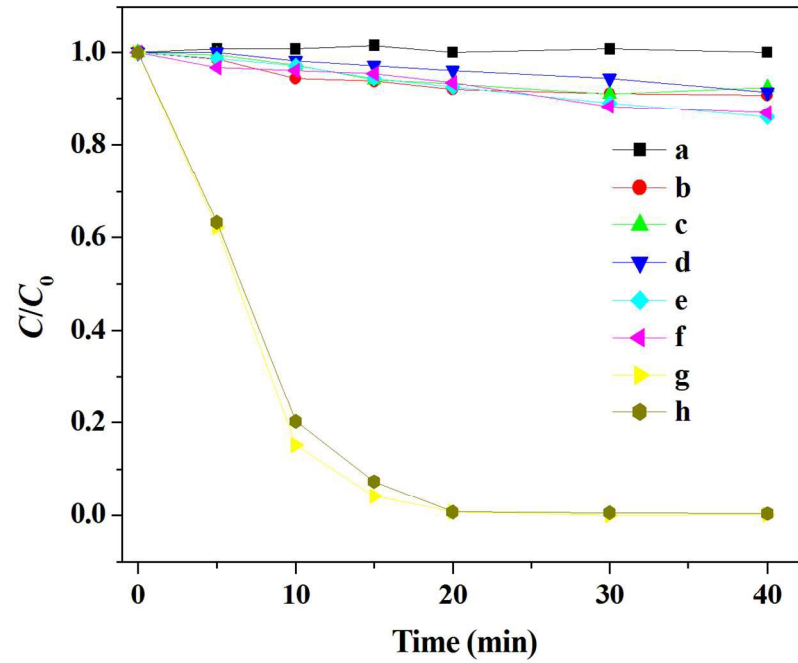
Fig.7 Degradation of RhB over the MOF 235 photocatalysts under different catalytic conditions.
279x215mm (150 x 150 DPI)
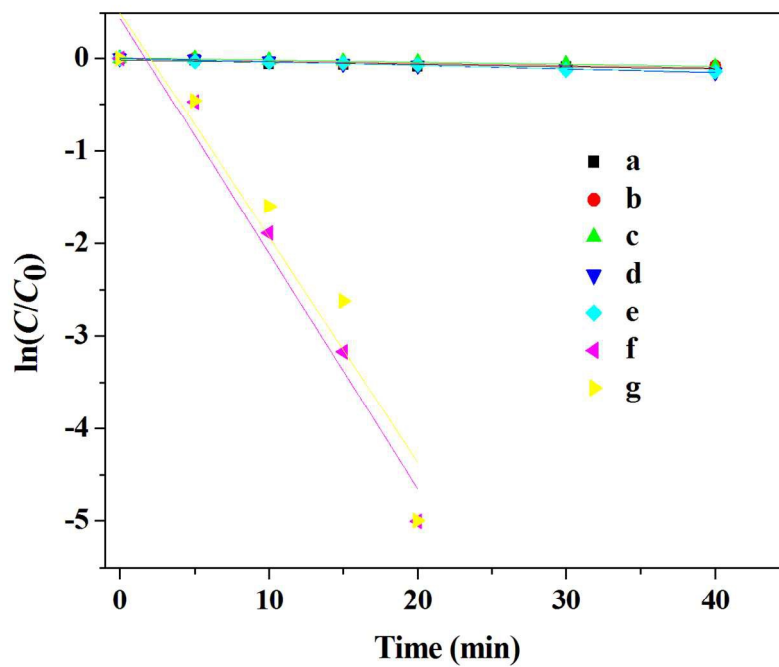
Fig.8 The reaction kinetics of RhB over the MOF 235 photocatalyst under different catalytic conditions.
279x215mm (150 x 150 DPI)
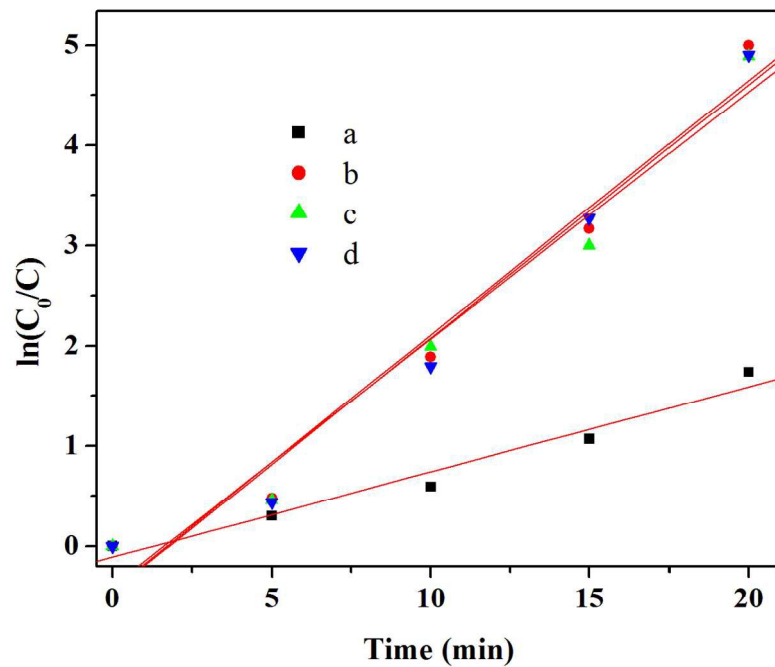
Fig.9 Photodegradation of RhB with MOF 235 phocatalyst in the presence of various amounts of H2O2 under visible light.
279x215mm (150 x 150 DPI)
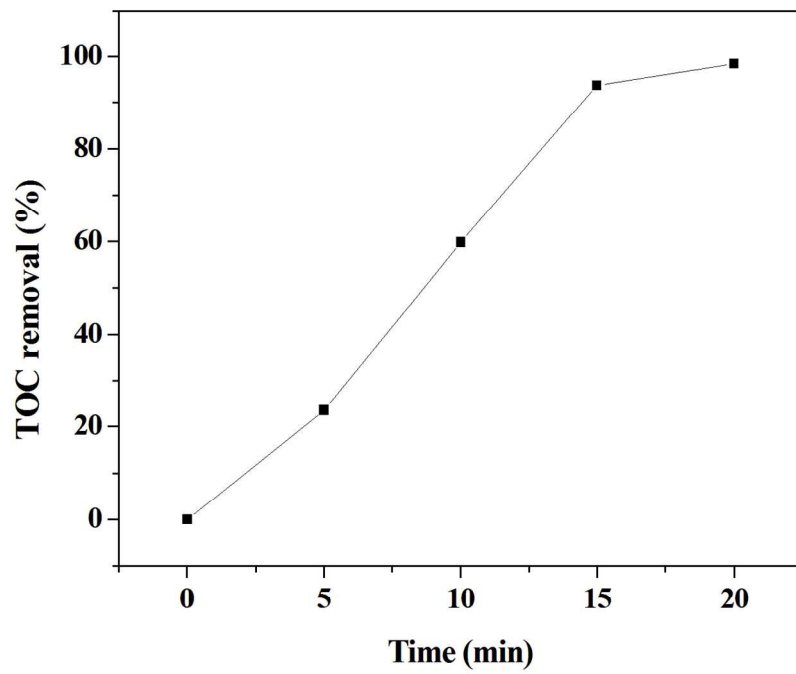
Fig.10 TOC removal yield of degraded bulk solution during the photocatalytic degradation of RhB under visible light.
279x215mm (150 x 150 DPI)
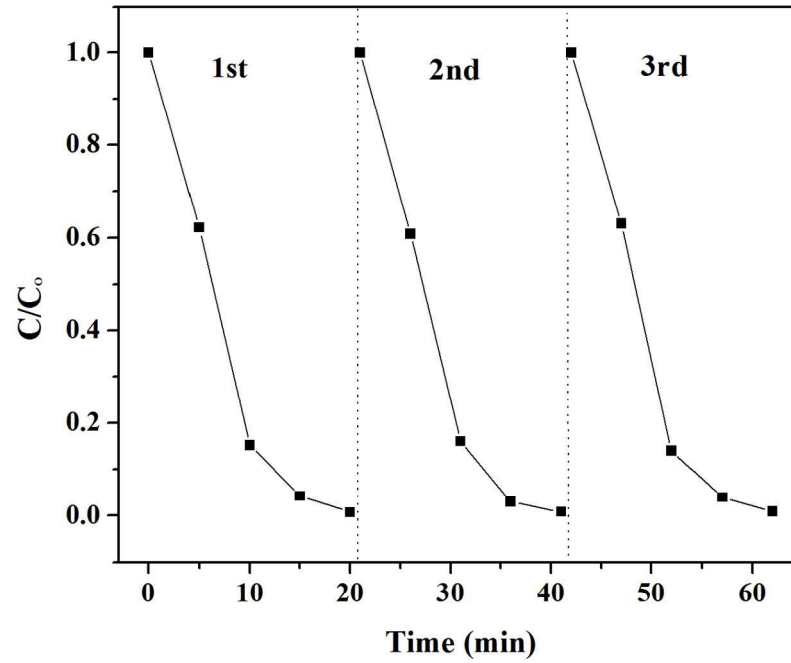
Fig.11 The photocatalytic RhB decolorization during three consecutive runs over MA-MOF 235/H2O2/visible light system.
279x215mm (150 x 150 DPI)
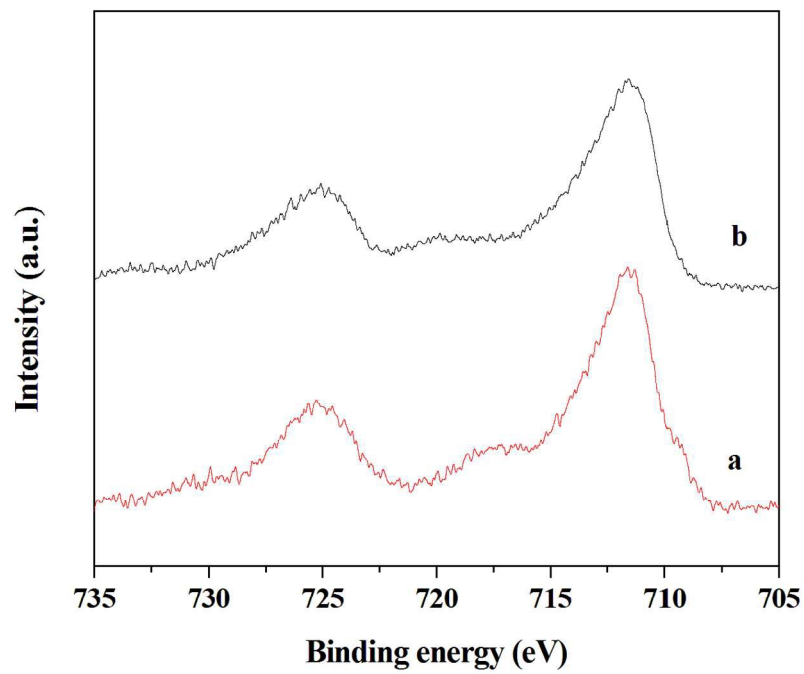
Fig.12 XPS spectrum of MA-MOF 235 (a)before and (b)after repeated usages for RhB degradation.
279x215mm (150 x 150 DPI)

Highlights

- MOF 235 was fabricated by a facile microwave-assisted method.

- It showed excellent visible-light photocatalytic activity in the presence of H_2O_2.

- It displays a high chemical stability for repeated RhB degradation reactions.